JEM

Supplemental material

Moeller et al., **https://doi.org/10.1084/jem.20182244**

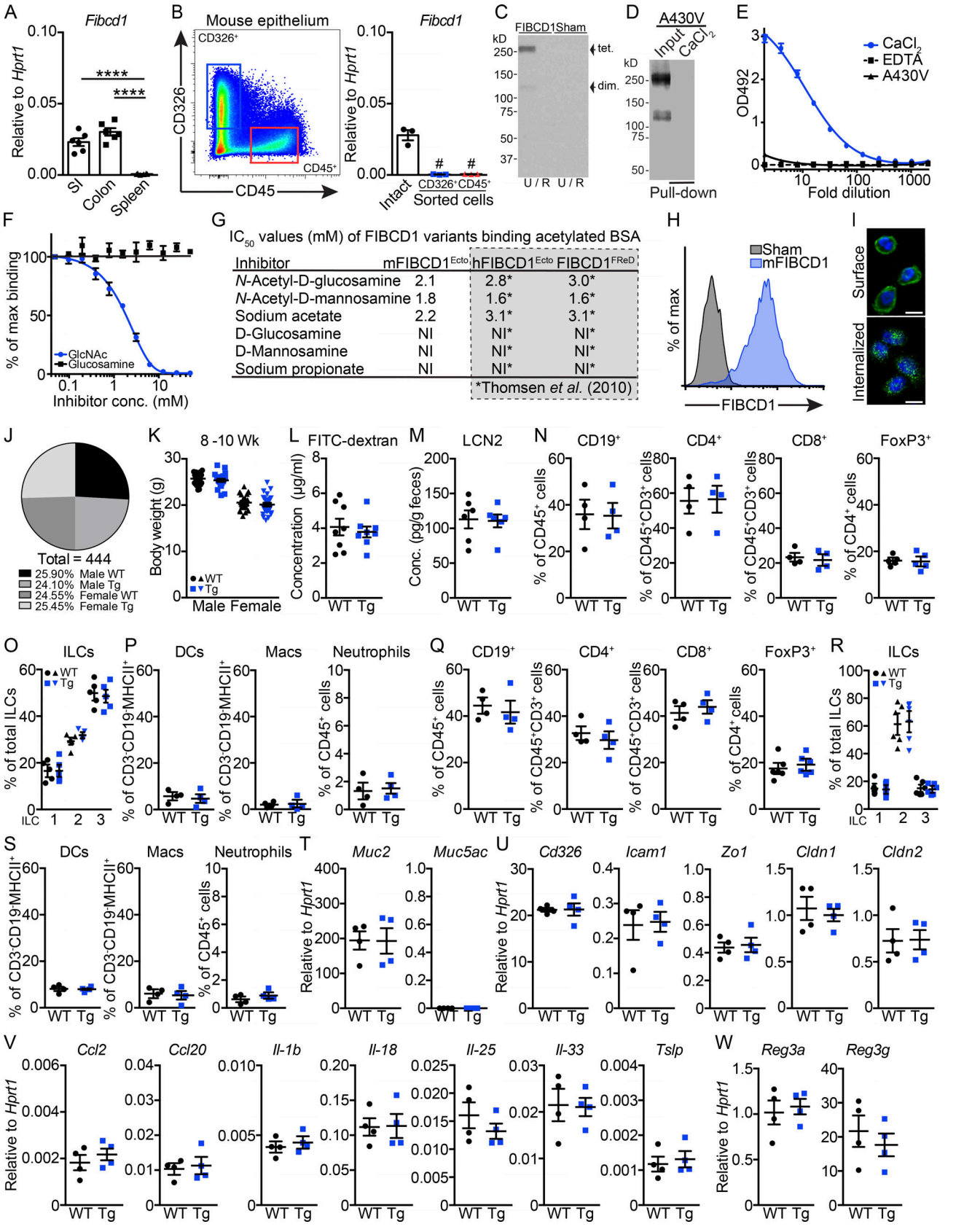
A
Fibcd1
Relative to Hprt1
0.10
0.05
0.00
****
****
SI
Colon
Spleen
B
Mouse epithelium
CD326+
CD326
CD45+
CD45
Fibcd1
Relative to Hprt1
#
#
Intact
CD326+CD45+
Sorted cells
C
FIBCD1Sham
kD
250-
150-
100-
75-
50-
37-
tet.
dim.
U / R U / R
D
A430V
Input
CaCl2
kD
250-
150-
100-
75-
50-
Pull-down
E
CaCl2
EDTA
A430V
OD492
Fold dilution
10
100
1000
F
% of max binding
100
50
0
GlcNAc
Glucosamine
0.1
1
10
Inhibitor conc. (mM)
G
IC50 values (mM) of FIBCD1 variants binding acetylated BSA
Inhibitor
mFIBCD1Ecto
hFIBCD1Ecto
FIBCD1FReD
N-Acetyl-D-glucosamine 2.1 2.8* 3.0*
N-Acetyl-D-mannosamine 1.8 1.6* 1.6*
Sodium acetate 2.2 3.1* 3.1*
D-Glucosamine NI NI* NI*
D-Mannosamine NI NI* NI*
Sodium propionate NI NI* NI*
*Thomsen et al. (2010)
H
Sham
mFIBCD1
% of max
FIBCD1
I
Surface
Internalized
J
Total = 444
25.90% Male WT
24.10% Male Tg
24.55% Female WT
25.45% Female Tg
K
8 -10 Wk
Body weight (g)
WT
Tg
Male Female
L
FITC-dextran
Concentration (µg/ml)
WT Tg
M
LCN2
Conc. (pg/g feces)
WT Tg
N
CD19+
CD4+
CD8+
FoxP3+
% of CD45+ cells
% of CD45+CD3+ cells
% of CD4+ cells
WT Tg
O
ILCs
% of total ILCs
ILC 1 2 3
P
DCs
Macs
Neutrophils
% of CD3-CD19-MHCII+
% of CD45+ cells
Q
CD19+
CD4+
CD8+
FoxP3+
R
ILCs
S
DCs
Macs
Neutrophils
T
Muc2
Muc5ac
Relative to Hprt1
U
Cd326
Icam1
Zo1
Cldn1
Cldn2
V
Ccl2
Ccl20
Il-1b
Il-18
Il-25
Il-33
Tslp
W
Reg3a
Reg3g

Figure S1. **Characterization of mouse FIBCD1 and *Fibcd1*^{Tg} mice. (A)** Expression of *Fibcd1* mRNA in SI, colon, and spleen from C57BL/6J mice (n = 6 samples per group). **(B)** Gating strategy and analysis of *Fibcd1* expression in CD45$^+$ and CD326$^+$ sorted cells, isolated from mouse colon (n = 3 samples per group). #, below the limit of detection. **(C)** Representative Western blot of recombinant mFIBCD1^{Ecto}. U, unreduced; R, reduced; tet., tetramer; dim., dimer. **(D)** Representative pull-down experiment demonstrating that mutation of Alanine^{430} to Valine^{430} (A430V), an essential amino acid located in the S1 acetyl-group binding pocket (Schlosser et al., 2009; Thomsen et al., 2010; Shrive et al., 2014), abolishes binding of mFIBCD1^{Ecto} to chitin. **(E)** Representative ELISA-based setup demonstrating Ca^{2+}-specific binding of mFIBCD1^{Ecto} to acetylated bovine serum albumin (acBSA). Mutation of A430V abolishes binding (average shown, technical triplicate). **(F)** Representative ELISA-based setup demonstrating acetyl group–specific inhibition of binding between mFIBCD1^{Ecto} and acBSA. GlcNAc inhibits binding, while nonacetylated glucosamine does not (average shown, technical triplicate). **(G)** Comparison of various acetylated molecules and their ability to inhibit binding between FIBCD1 variants and acetylated BSA by 50%. Inhibitory concentration 50% (IC_{50}). No apparent difference in inhibition observed between mFIBCD1^{Ecto} (used in this study) vs. human FIBCD1^{Ecto} or truncated fibrinogen-related domain FIBCD1^{FReD} (97% identity between human and mouse) reported by Thomsen et al. (2010). NI, not inhibitory. **(H)** Representative histograms of full-length mFIBCD1 surface expressed on HEK293 cells. **(I)** Representative fluorescence imaging of full-length recombinant mFIBCD1 expressed on HEK293 cells. Blue, DAPI; green, FIBCD1. Membrane-bound at 4°C (upper panel), but internalized at 37°C (lower panel). Scale bars: 20 µm. **(J)** Distribution of sex and genotype from breeding of *Fibcd1*^{Tg} (Tg) and WT mice (444 mice in total). **(K)** Assessment of body weight in 8–10-wk-old WT and Tg littermates (n = 22–26 mice per group). **(L)** Intestinal barrier integrity and permeability assessed by FITC-dextran feeding of WT and Tg littermates (n = 8 samples per group). **(M)** Analysis of Lipocalin-2 (LCN2) levels in feces (n = 6 samples per group). **(N–S)** Frequencies of CD19$^+$ B cells, CD4$^+$ and CD8$^+$ T cells, FoxP3$^+$ regulatory T cells, ILCs, CD11c$^+$CD64$^-$ dendritic cells (DCs), CD64$^+$ macrophages (Macs), and Ly6G$^+$ neutrophils isolated from small intestinal LP (N–P) and colon LP (Q–S) of WT and Tg littermates (n = 4 samples per group). Total ILCs defined as live CD45$^+$CD11b$^-$CD11c$^-$B220$^-$CD3$^-$CD5$^-$FcεRI$^-$CD90$^+$CD127$^+$ cells. ILC subsets defined as GATA3$^-$RORγt$^-$Tbet$^+$ (ILC1s), RORγt$^-$GATA3$^+$ (ILC2s), and GATA3$^-$RORγt$^+$ (ILC3s). **(T–W)** mRNA expression of *Muc2*, *Muc5ac*, *Cd326*, *Icam1*, *Zo1*, *Cldn1*, *Cldn2*, *Ccl2*, *Ccl20*, *Il1b*, *Il18*, *Il25*, *Il33*, *Tslp*, *Reg3a*, and *Reg3g*, genes associated with epithelial barrier integrity and immunity in sorted (Live CD45$^-$CD326$^+$) colonic epithelial cells from of WT and Tg littermates (n = 4 or 5 samples per group). Results shown in A–I are representative of at least three independently performed experiments with similar results. Results shown in J and K are pooled data from 67 independent litters and eight independently performed experiments, respectively. Results shown in L–W are representative of at least two independently performed experiments with similar results. Statistics: Data are presented as mean ± SEM where dots represent individual mice. One-way ANOVA followed by Tukey post hoc test was used to analyze data in A, two-way ANOVA followed by Holm–Sidak post hoc test was used to analyze results in K, and unpaired Student's t test was used to analyze data in L–W. ****, $P < 0.0001$. Conc., concentration; max, maximum.

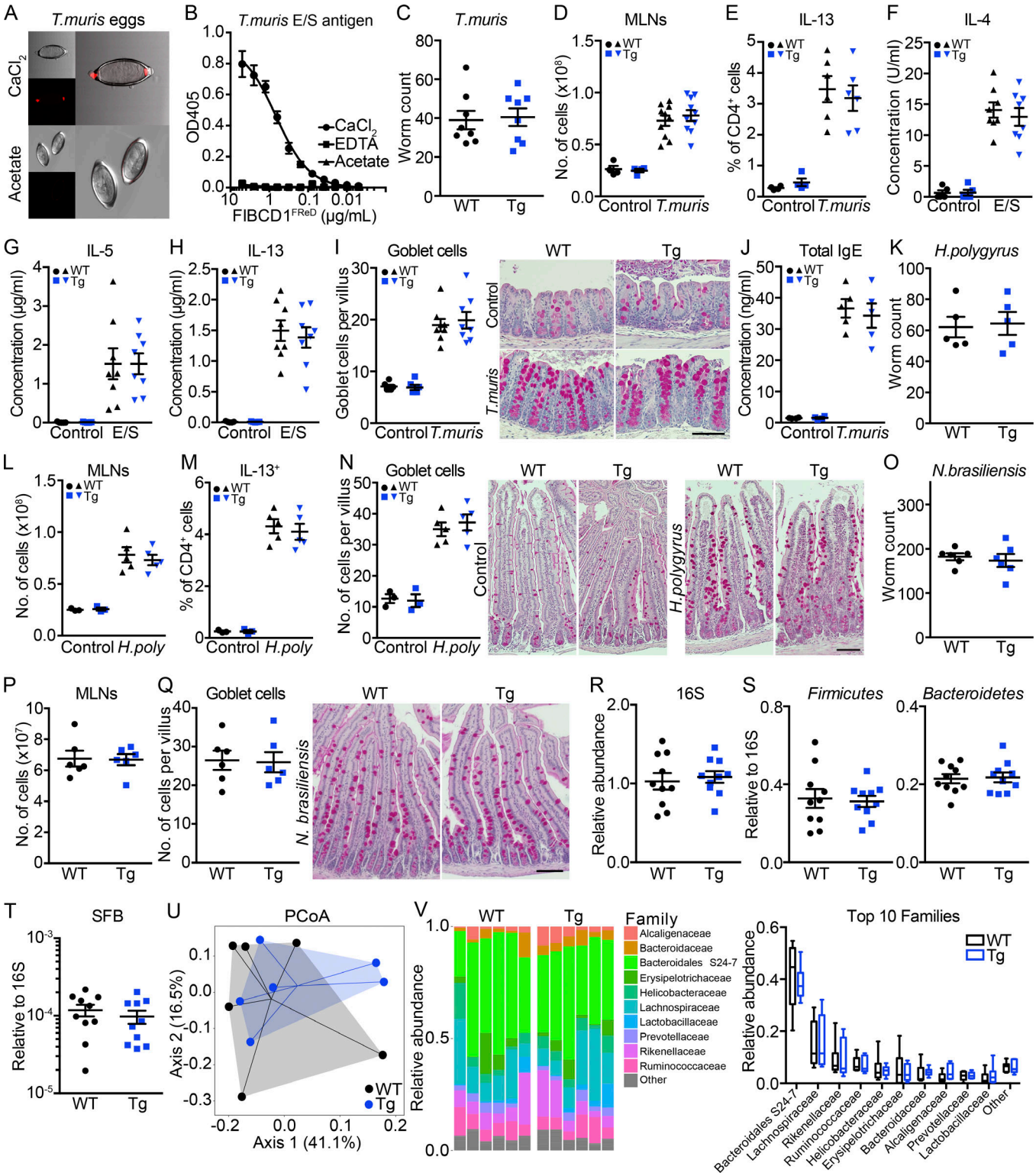
A
T.muris eggs
CaCl2
Acetate
B
T.muris E/S antigen
OD405
CaCl2
EDTA
Acetate
FIBCD1FReD (µg/mL)
C
T.muris
Worm count
WT
Tg
D
MLNs
No. of cells (x10⁶)
Control T.muris
E
IL-13
% of CD4+ cells
Control T.muris
F
IL-4
Concentration (U/ml)
Control E/S
G
IL-5
Concentration (µg/ml)
Control E/S
H
IL-13
Concentration (µg/ml)
Control E/S
I
Goblet cells
Goblet cells per villus
Control T.muris
WT
Tg
J
Total IgE
Concentration (ng/ml)
Control T.muris
K
H.polygyrus
Worm count
L
MLNs
No. of cells (x10⁶)
Control H.poly
M
IL-13+
% of CD4+ cells
Control H.poly
N
Goblet cells
No. of cells per villus
Control H.poly
H.polygyrus
O
N.brasiliensis
Worm count
P
MLNs
No. of cells (x10⁷)
Q
Goblet cells
No. of cells per villus
N. brasiliensis
R
16S
Relative abundance
S
Firmicutes
Bacteroidetes
Relative to 16S
T
SFB
Relative to 16S
U
PCoA
Axis 2 (16.5%)
Axis 1 (41.1%)
V
Family
Alcaligenaceae
Bacteroidaceae
Bacteroidales S24-7
Erysipelotrichaceae
Helicobacteraceae
Lachnospiraceae
Lactobacillaceae
Prevotellaceae
Rikenellaceae
Ruminococcaceae
Other
Relative abundance
Top 10 Families
Bacteroidales S24-7
Lachnospiraceae
Rikenellaceae
Ruminococcaceae
Helicobacteraceae
Erysipelotrichaceae
Bacteroidaceae
Alcaligenaceae
Prevotellaceae
Lactobacillaceae
Other

Figure S2. **FIBCD1 does not modulate immunity to helminth infection nor changes the composition of gut bacteria. (A–J)** Characterization of FIBCD1 in the *T. muris* helminth model. **(A)** Representative fluorescence imaging of Alexa Fluor 647–labeled recombinant FIBCD1^{FReD} binding (red) to the chitin-rich polar plugs of *T. muris* eggs (upper panel). Binding is abolished by acetylated structures such as acetate (lower panel). **(B)** Representative ELISA-based setup demonstrating Ca^{2+}-dependent binding of recombinant FIBCD1 to *T. muris* E/S antigen (mean shown, technical triplicate). **(C)** *T. muris* worm burden assessed at day 18 in large intestine after infecting WT and *Fibcd1*^{Tg} (Tg) littermates with 200 embryonated eggs by oral gavage (n = 8 mice per group). **(D)** Absolute cell numbers in MLNs in naive and *T. muris*–infected mice (n = 4–10 samples per group). **(E)** Analysis by flow cytometry of IL-13–producing CD4$^+$ T cells isolated from MLNs (n = 4–6 samples per group). **(F–H)** Secretion of IL-4, IL-5, and IL-13 by cultured MLN cells restimulated with *T. muris* E/S antigen (n = 5–8 samples per group). **(I)** Quantification of goblet cell hyperplasia after *T. muris* infection (n = 6–8 samples per group). Representative PAS stains of cecal tissues are depicted. Scale bar, 100 µm. **(J)** Assessment of total IgE antibody responses 18 d after infection (n = 3–5 samples per group). **(K–N)** Characterization of FIBCD1 in the *H. polygyrus* (*H. poly*) helminth model. **(K)** *H. polygyrus* worm burden in the intestine assessed at day 18 after infecting WT and Tg littermates with 200 infective L3 larvae by oral gavage (n = 5 mice per group). **(L)** Absolute cell numbers in the MLNs (n = 3–5 sample per group). **(M)** Analysis by flow cytometry of IL-13–producing CD4$^+$ T cells isolated from MLNs (n = 3–5 samples per group). **(N)** Quantification of goblet cell hyperplasia after *H. polygyrus* infection (n = 3–5 samples per group). Representative PAS stains of duodenal tissues are depicted. Scale bar, 100 µm. **(O–Q)** Characterization of FIBCD1 in the *N. brasiliensis* helminth model. **(O)** *N. brasiliensis* worm burden in the SI assessed at day 7 after infecting WT and Tg littermates with 500 infective L3 larvae by subcutaneous injection (n = 5 mice per group). **(P)** Absolute cell numbers in the MLNs (n = 5 samples per group). **(Q)** Quantification of goblet cell hyperplasia after *N. brasiliensis* infection (n = 5 samples per group). Representative PAS stains of duodenal tissues are depicted. Scale bar, 100 µm. **(R–V)** Assessment of gut bacteria by qPCR and 16S sequencing. **(R)** Abundance of intestinal bacteria as determined by 16S qPCR in WT and Tg littermates (n = 10 samples per group). **(S)** Relative abundance of the two major bacterial phyla (Firmicutes and Bacteroidetes) after normalization to total 16S bacteria (n = 10 samples per group). **(T)** Relative abundance of segmented filamentous bacteria (SFB) normalized to 16S (n = 10 samples per group). **(U and V)** 16S sequencing of fecal DNA collected from WT and Tg littermates cohoused until 6 wk of age then housed two additional weeks based on genotype. **(U)** PCoA ordination based on Bray–Curtis dissimilarities in colonic bacterial OTUs (n = 6 samples per group). **(V)** Relative abundance of the 10 major bacterial families; error bars represent minimum-maximum (n = 6 samples per group). Data shown in A–E and R–T are representative of at least three independently performed experiments with similar results. Results in F–J are pooled from two independently performed experiments. Data in K–Q are representative of at least two independently performed experiments with similar results. Data in U and V are pooled results from two independent cages per group. Statistics: Data are presented as mean ± SEM where dots represent individual mice. Unpaired Student's *t* test was used to analyze results in C, K, and O–T, and two-way ANOVA followed by Holm–Sidak post hoc test was used to analyze data in D–J and L–N.

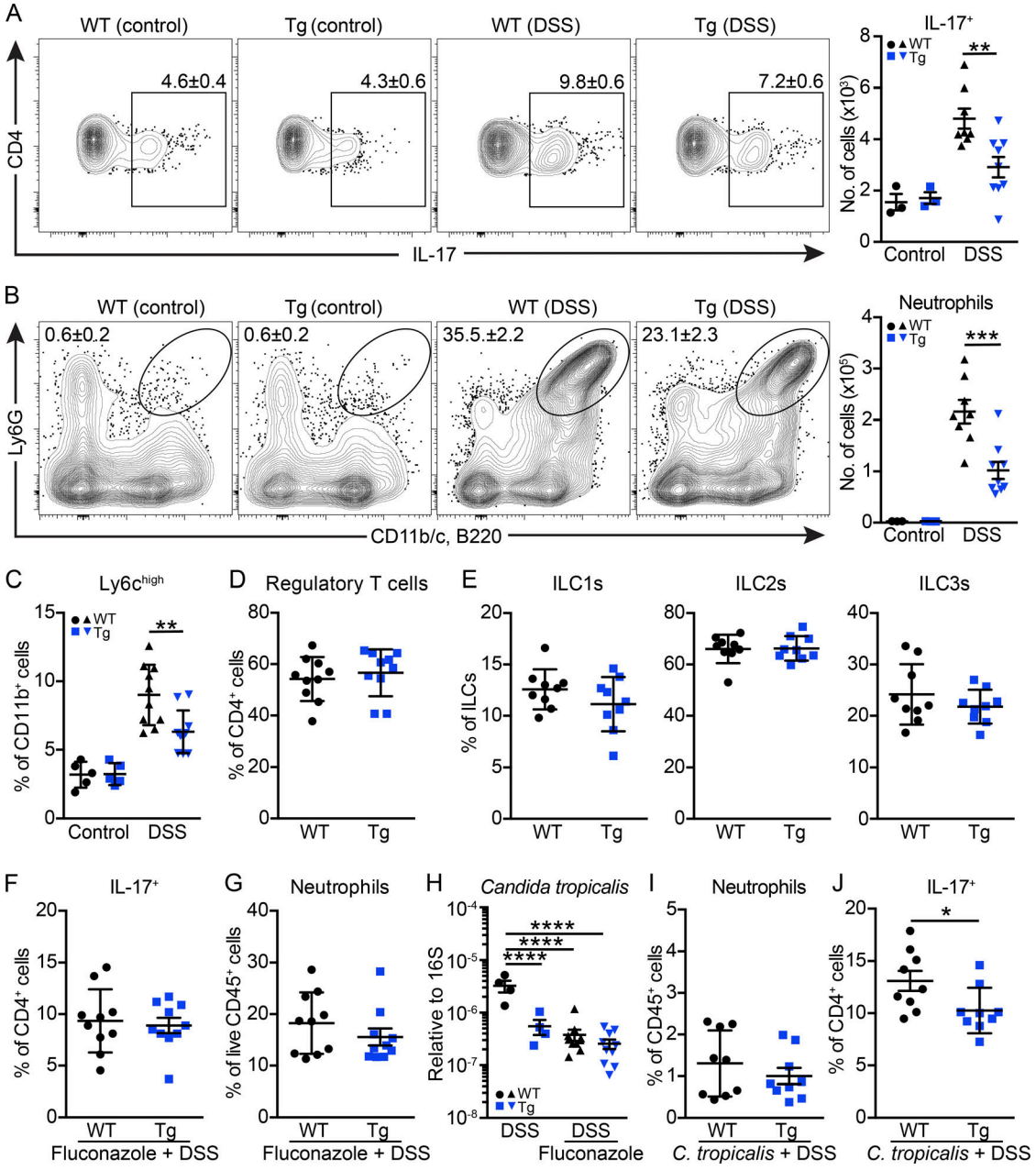

Figure S3. **Quantification of immune cell composition and fungi in DSS-driven intestinal inflammation. (A–E)** WT and *Fibcd1*^{Tg} (Tg) littermates were exposed to 2.5% (wt/vol) DSS in the drinking water for 7 d followed by 3 d of regular water. **(A)** Scatter plots and absolute numbers of $CD45^+CD3^+CD4^+IL\text{-}17^+$ T cells in the colon LP (n = 3–9 samples per group). **(B)** Scatter plots and absolute numbers of infiltrating $CD45^+CD11b^+Ly6G^+$ neutrophils in the colon LP population (n = 3–9 samples per group). **(C)** Frequencies of infiltrating live $CD45^+CD11b^+Ly6c^{high}$ inflammatory monocytes in the colon LP (n = 4–10 samples per group). **(D)** Frequencies of live, $CD45^+CD4^+FoxP3^+$ regulatory T cells in the colon LP after exposure to DSS (n = 10 samples per group). **(E)** Frequencies of ILCs in the colon LP after DSS exposure (n = 9 samples per group). Total ILCs defined as live $CD45^+CD11b^-CD11c^-B220^-CD3^-CD5^-Fc\varepsilon RI^-CD90^+CD127^+$ cells. ILC subsets defined as $GATA3^-ROR\gamma t^-Tbet^+$ (ILC1s), $ROR\gamma t^-GATA3^+$ (ILC2s), and $GATA3^-ROR\gamma t^+$ (ILC3s). **(F–H)** WT and Tg littermates treated with fluconazole before being exposed to 2.5% (wt/vol) DSS in the drinking water. Fluconazole treatment (0.5 g/liter in drinking water) was initiated day −3 and maintained throughout the experiment. **(F)** Frequencies of $CD45^+CD3^+CD4^+IL\text{-}17^+$ T cells in the colon LP at time of sacrifice (n = 10 samples per group). **(G)** Frequencies of infiltrating $CD45^+CD11b^+Ly6G^+$ neutrophils in the colon LP at time of sacrifice (n = 10 samples per group). **(H)** Quantification of the relative abundance of *C. tropicalis* in fluconazole-treated mice after DSS exposure (n = 4–10 samples per group). **(I and J)** WT and Tg littermates were colonized with *C. tropicalis* as described in Fig. 3 A before being exposed to 2.5% (wt/vol) DSS in the drinking water. **(I)** Frequencies of infiltrating $CD45^+CD11b^+Ly6G^+$ neutrophils in the colon LP after 6 d of DSS exposure (n = 9 samples per group). **(J)** Frequencies of $CD45^+CD3^+CD4^+IL\text{-}17^+$ T cells in the colon LP after 6 d of DSS exposure (n = 9 sample per group). Data shown in A and B are representative of three independently performed experiments. Results shown in C–E are representative of two independently performed experiments. Data shown in F–J are pooled results from two independently performed experiments. Statistics: Data are presented as mean ± SEM where dots represent individual mice. Two-way ANOVA followed by Holm–Sidak post hoc test was used to analyze results in A–C and H, and unpaired Student's t test was used to analyze results in D–G, I, and J. *, $P < 0.05$, **, $P < 0.01$, ***, $P < 0.001$, and ****, $P < 0.0001$.

References

Schlosser, A., T. Thomsen, J.B. Moeller, O. Nielsen, I. Tornøe, J. Mollenhauer, S.K. Moestrup, and U. Holmskov. 2009. Characterization of FIBCD1 as an acetyl group-binding receptor that binds chitin. *J. Immunol.* 183:3800–3809. https://doi.org/10.4049/jimmunol.0901526

Shrive, A.K., J.B. Moeller, I. Burns, J.M. Paterson, A.J. Shaw, A. Schlosser, G.L. Sorensen, T.J. Greenhough, and U. Holmskov. 2014. Crystal structure of the tetrameric fibrinogen-like recognition domain of fibrinogen C domain containing 1 (FIBCD1) protein. *J. Biol. Chem.* 289:2880–2887. https://doi.org/10.1074/jbc.M113.520577

Thomsen, T., J.B. Moeller, A. Schlosser, G.L. Sorensen, S.K. Moestrup, N. Palaniyar, R. Wallis, J. Mollenhauer, and U. Holmskov. 2010. The recognition unit of FIBCD1 organizes into a noncovalently linked tetrameric structure and uses a hydrophobic funnel (S1) for acetyl group recognition. *J. Biol. Chem.* 285:1229–1238. https://doi.org/10.1074/jbc.M109.061523